ELSEVIER

Polymer 42 (2001) 2067–2075

polymer

www.elsevier.nl/locate/polymer

Epoxy + liquid crystalline epoxy coreacted networks: I. Synthesis and curing kinetics

P. Punchaipetch[a], V. Ambrogi[a,b], M. Giamberini[b], W. Brostow[a], C. Carfagna[b], N.A. D'Souza[a,*]

[a]*Department of Materials Science, University of North Texas, Denton, TX 76203-5310, USA*
[b]*Department of Materials and Production Engineering, University of Naples "Federico II", Piazzale Tecchio 80, 80125 Naples, Italy*

Received 13 December 1999; received in revised form 5 June 2000; accepted 13 June 2000

Abstract

In situ copolymerization of diglycidyl ether of 4,4′-dihydroxybiphenol (DGE-DHBP) with diglycidyl ether of bisphenol F (DGEBP-F) networks using an anhydride curing agent has been investigated. DGEBP-F is a commercial epoxy while cured DGE-DHBP shows liquid crystal transitions. Curing kinetics are determined using differential scanning calorimetry (DSC). The data were fitted using an autocatalytic curing model for both pure and mixed components. Isothermal and non-isothermal methods were compared. The glass transition (T_g) was evaluated as a function of composition using DSC. The results show that the DGE-DHBP constituent affects the curing kinetics of the epoxy resin and that the network exhibits one T_g. © 2000 Published by Elsevier Science Ltd.

Keywords: Epoxy resin; Liquid crystalline epoxy resin; Curing kinetics

1. Introduction

Epoxy resins are used in many applications because of their high strength, stiffness, good thermal stability, and excellent adhesion properties. Unfortunately, they also have low fracture toughness. Two common approaches for epoxy modifications are introduction of functionalized reactive rubbers or thermoplastics. Reactive rubbers like carboxyl- (CTBN), amine- (ATBN) or epoxy-terminated butadiene acrylonitrile (ETBN) have improved toughness. However, the blends show adverse effects on glass transition temperature range, stiffness and strength [1–3]. The mechanism of toughening of such blends involves a chemically induced phase separation process [4]. Toughening epoxies with thermoplastics presents significant problems in processing due to the large viscosity difference between the thermoplastics and the epoxy. One of us showed that interpenetrating networks (IPNs) formed through simultaneous reaction of an epoxy and polyisocyanate monomer in the presence of a single curing agent increased fracture toughness [5]. Controlling the phase separation has been approached through simultaneous curing of the epoxy resin with rubbery networks to form an IPN [6].

Liquid crystalline epoxy (LCE) networks are an important area of research given their potential use in a number of applications such as electronics, advanced composites, non-linear optics, etc. The synthesis, development of texture, mechanical properties and influence of curing conditions have been examined for a number of LCEs [7–21]. Given the considerable interest in blending thermotropic longitudinal polymer liquid crystals (PLCs) with other thermoplastics to improve mechanical properties of thermoplastics [22–27], there has been some interest in examining the case of PLCs + thermosets [18,28].

Liquid crystalline thermosets and particularly LCE resins show interesting properties due to the combination of a thermoset and LC formation capability [29–34]. As compared to ordinary epoxies, crosslinked LCEs exhibit higher fracture toughness [32,35] and mechanical properties when oriented by magnetic fields [36]. It should be noted that all PLCs, including those derived from diglycidyl-terminated blocks, are characterized by repetitive units that are highly anisotropic, where the molecular structure determines the appearance of LC state [37].

In the past, polyfunctional amines and aliphatic diacids were widely used to cure LC epoxies [18,32–35]. Here we opt for an anhydride curing agent because of the good thermal stability, electrical insulation, and relatively high chemical resistance. Furthermore, anhydride curing agents provide good mechanical properties with low shrinkage so they are suitable for matrices in composite applications [38].

* Corresponding author. Tel.: +1-940-565-2979; fax: +1-940-565-4824.
E-mail address: ndsouza@jove.unt.edu (N.A. D'Souza).

0032-3861/01/$ - see front matter © 2000 Published by Elsevier Science Ltd.
PII: S0032-3861(00)00505-X

The mechanisms of catalyzed cure of epoxies with cyclic anhydrides involve an anionic mechanism suggested by Fisher [39]. The reaction is supposed to occur via a formation of a zwitterion. A tertiary amine first reacts with the anhydride group to create the carboxylate zwitterion group [$[R'_3N^{\oplus}$-CO-CO-$O^{\ominus}$].]. Then, the reactive groups can react further with an epoxide. Tanaka and Kakiuchi [40] suggested that a tertiary amine in the form of hydroxylate [$R_3N^{\oplus}CH_2$–$CH(CH_2R')O^{\ominus}$] can also react with anhydride groups.

In this paper we investigate the effect of coreacting a conventional epoxy resin with a diglycidyl-terminated liquid crystalline monomer. Synthesis, curing kinetics and degree of miscibility of the resulting system are reported in Part I. Part II deals with the effects of modified epoxy on the mechanical performance.

2. Kinetics of curing: models

DSC is extensively used for investigating the curing reaction of thermoset polymers. Kinetics can be characterized with DSC by measuring heat generated during the curing reaction as a function of temperature and time. The extent of curing reaction may be determined by measuring the total area of the reaction peak. The basic assumption of DSC kinetic measurements is that the heat flow is proportional to the change in the extent of the reaction:

$$\alpha = \frac{d\alpha}{dt} = \frac{1}{H_{tot}} \frac{dH}{dt} \tag{1}$$

where dH/dt represents the rate of heat generated during curing reaction. H_{tot} is the overall heat of reaction and α is the extent of reaction while $d\alpha/dt$ is the rate of the reaction.

Several different kinetic models have been used to characterize curing of epoxy resin by relating the chemical reactions to time, temperature and extent of cure [41]. The simplest expression is the *n*th-order model as shown in Eq. (2).

$$\frac{d\alpha}{dt} = k(1-\alpha)^n \tag{2}$$

where n is the reaction order, and k represents the rate constant. In turn, one often represents k by an Arrhenius type formula:

$$k = k_0 \exp(-E_a/RT) \tag{3}$$

where k_0 is the Arrhenius frequency factor, E_a is the activation energy, R is the gas constant, and T is absolute temperature.

The isothermal thermogram from the *n*th-order reaction predicts the maximum reaction rate at time equal to zero. However, this model cannot be applied to the entire reaction because of complex cure mechanisms. The existence of impurities or catalysts in amine or anhydride curing agents does not necessarily preclude the reaction following the autocatalytic model; however, more complex mechanisms are also possible [42]. If an isothermal process characterized by a thermogram shows a maximum reaction rate at some point other than the start of the reaction, an autocatalytic model given below (Eq. (4)) has been found to be more appropriate to investigate kinetic parameters. Prime pointed out that the curing reaction of a thermoset was not limited to one chemical reaction. Two or more consecutive curing reactions are possible as investigated by Lau [43]. He found that the cure of an amine system at room temperature proceeded first from combined *n*th-order and autocatalytic models, then predominantly by autocatalytic models. Finally, the reaction became diffusion controlled as T_g increased to 10–15°C above curing temperature.

In this study, the kinetic parameters were calculated based on a two-parameter autocatalytic model. Kamal and co-workers [44,45] proposed a generalized model, which gives a description of curing up to the vitrification point as follows:

$$\frac{d\alpha}{dt} = (k_1 + k_2\alpha^m)(1-\alpha)^n \tag{4}$$

where k_1 is the externally catalyzed rate constant, and k_2 is the autocatalyzed rate constant with Arrhenius temperature dependency.

The cure mechanism is assumed to be the same for the entire temperature range investigated. Therefore, the constant k_1 is calculated using the initial reaction rate at $t = 0$ from the intercept of the isothermal thermogram. Consequently, Eq. (4) is simplified to

$$\left.\frac{d\alpha}{dt}\right|_{t=0} = k_1 \tag{5}$$

The kinetics can be investigated by dynamic experiments at different heating rates and applied to the Kissinger method [46]. The activation energy can be calculated from the following equation:

$$\frac{d[\ln(\varphi/T_m^2)]}{d[1/T_m]} = -\frac{E_a}{R} \tag{6}$$

where φ represents dT/dt or the heating rate, and T_m is the peak temperature.

3. Experimental

3.1. Materials

The epoxy resin used in this study is a low-viscosity diglycidyl ether of bisphenol F (DGEBP-F) (Shell EPON862®) with the epoxide equivalence weight (EEW) in the range 166–177. DGEBP-F will be named as EP_1 for convenience. Methyltetrahydrophthalic (MTHPA) anhydride (Lindride-6®) pre-catalyzed by benzyl triethyl ammonium chloride (BTEAC) is the curing agent obtained

pre-mixed from Lindau Chemical. Its anhydride equivalent weight is in the range 165–175. The formula of DGEBP-F and MTHPA are shown below:

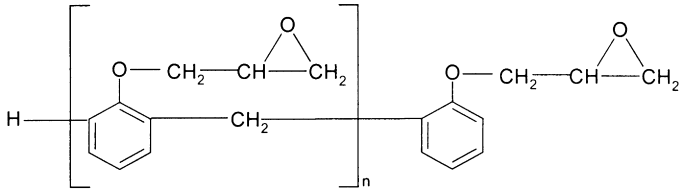

DGEBP-F (EP_1)

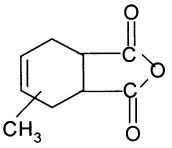

MTHPA

The epoxy monomer with the capability of forming LC phase is the diglycidyl ether of 4,4′-dihydroxybiphenol (DGE-DHBP), which will be called *EP_2*. The formula and synthesis procedure of this monomer are described in Section 3.2.

3.2. Synthesis

EP_2 was synthesized by endcapping the hydroxyl groups of biphenol with epichlorohydrin in the presence of sodium hydroxide, as described by some of us [32]. The yield is about 60%. The scheme of the synthesis is as follows:

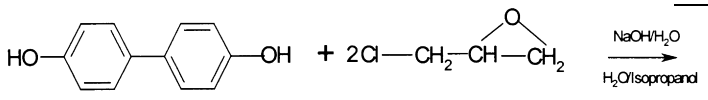

Biphenol Epichlorohydrin

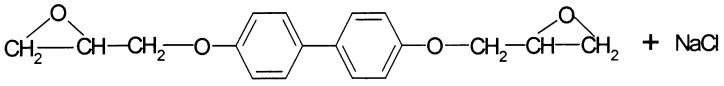

Diglycidyl ether of 4,4'-dihydroxybiphenol

(EP_2)

DGE-DHBP has the EEW of 166. The rigid rod length is about 0.72 nm [32]. The material was selected on the basis of the same EEW as the epoxy resin. The synthesized products were characterized by DSC, FT-IR, polarized optical microscope (POM) and X-ray diffraction (XRD) to determine the transition temperatures, functional groups, and liquid crystal properties. The polarized optical microscope used is Zeiss (Axioplan) equipped with camera and Ernst Leitz heating stage. After synthesis, EP_2 was dried for 48 h at 70°C under vacuum and ground to assure the homogeneous mixture with EP_1.

3.3. Differential scanning calorimetry (DSC)

The EP_1 and ground EP_2 were mixed well in a 1:1 molar ratio. Then, MTHPA was added in the stoichiometric ratio of 1:1 to the system. The mixture was mixed well at room temperature. The ratio was chosen on the basis of the approximately stoichiometric equivalence of EP_1 and EP_2. 10–15 mg of the sample were weighed into a high-pressure-sealed DSC pan and kept in the refrigerator before performing the DSC measurement. A Perkin–Elmer DSC7 apparatus was used. Isothermal experiments were conducted from 100 to 160°C at 10-K intervals for 250 min. Each sample was placed in a sample holder after the desired temperature was reached and then quenched to 25°C. A second scan was conducted from 25 to 250°C at the heating rate of 10 K/min to determine the glass transition temperature T_g and residual heat, if present. Nitrogen was the carrier gas with the flow rate of 30 ml/min. Non-isothermal experiments were conducted from 25 to 250°C at several heating rates: 1.5, 2.5, 5, 10, and 20 K/min. N_2 was used as the purge gas.

4. Results and discussion

4.1. Synthesis

The DSC thermogram of the synthesized EP_2 reveals a first transition at 135°C followed by the melting point at 158°C. The heats of transition were 20.5 and 73.7 J/g, respectively. Optical microscope shows that there is no change in the appearance of crystalline texture on low-temperature transition. The crystal melts and becomes isotropic upon heating at 157.8°C. Upon cooling to room

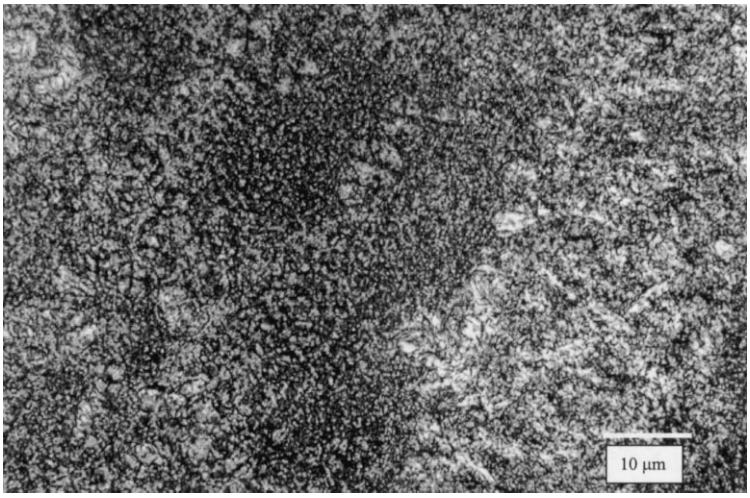

Fig. 1. The optical microscopy of DGE-DHBP cured with MTHPA under cross polarizers (magnification 40 ×).

temperature a double peak is recorded with the two maxima at 140 and 149°C, as also previously observed [47]. The LC phase has not been found for the uncured sample. This interpretation is based on the results of Hefner et al. [48] who reported the absence of the LC phase earlier. The nematic LC phase was formed during curing for DGE-DHBP and amine curing agent [32,47]. Fig. 1 shows the LC phase formed from EP_2 cured with MTHPA as seen in optical microscopy between crossed polarizers. The biphasic character, where the nematic phase is embedded

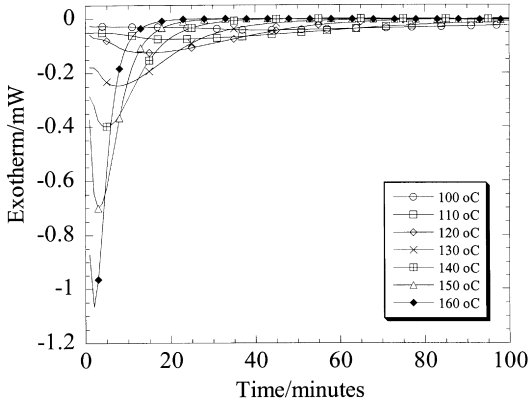

Fig. 2. An exotherm of the isothermal measurement for the DGEBP-F system.

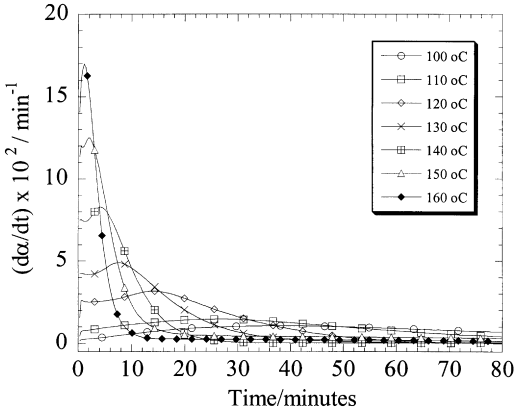

Fig. 4. Rates of cure vs. time at various temperatures as a function of time for DGE-DHBP + MTHPA.

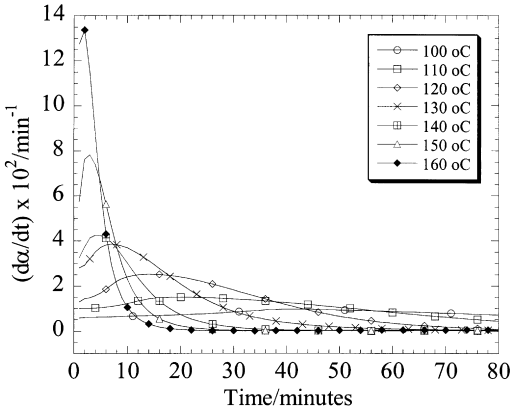

Fig. 3. Rates of cure as a function of time for the DGEBP-F + MTHPA.

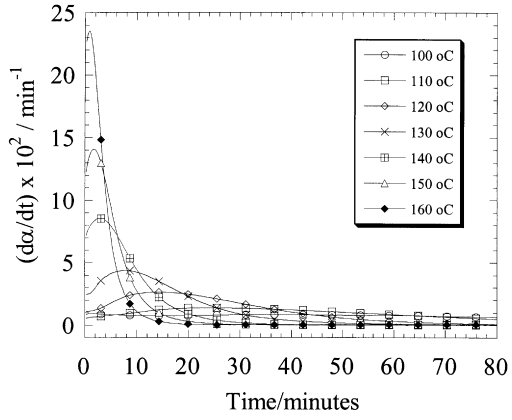

Fig. 5. Rates of cure vs. time at various temperature for blend of DGE-DHBP and DGEBP-F.

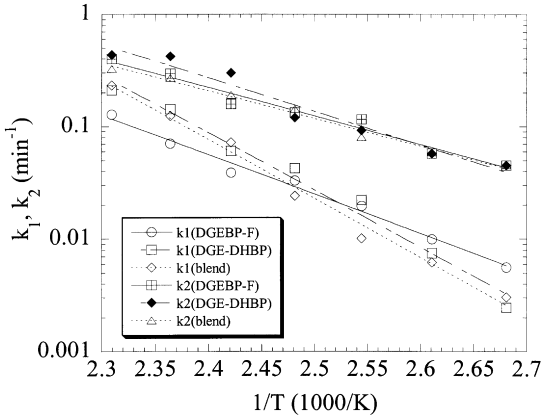

Fig. 6. Comparison of reaction rate for DGEBP-F, DGE-DHBP, and blend of DGEBP-F with DGE-DHBP.

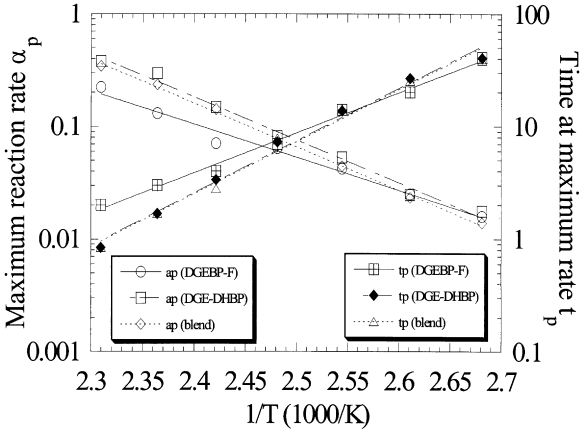

Fig. 7. Comparison of maximum reaction rate α_p (open symbols) and time to attain maximum rate t_α (filled symbols).

in the isotropic phase, is observed. We do not observe the LC formation for blend samples by POM. As the blend of EP_1 and EP_2 was heated, the LC component was melted and dissolved into the mixture. The functional groups of the product were checked by FT-IR measurement and followed during curing. The peak at 915 cm^{-1}, which represents the absorption related to the asymmetric stretch of epoxy ring, was monitored. This peak was examined in the cured samples to resolve the amount of epoxy left in the system.

4.2. Curing kinetics

The exotherms obtained by DSC for the mixture of EP_1 and MTHPA at several isothermal temperatures are reported in Fig. 2. A diagram of reaction rate as a function of curing time can therefore be obtained with the assumption that the heat generated during cure is directly proportional to the rate of reaction. The H_{tot} is calculated from the total area under the dynamic scan of curing thermogram at 10 K/min. The corresponding value for the EP_1 + MTHPA system is 315 J/g. The diagram shows autocatalytic kinetic behavior from the non-zero initial reaction rate. The rate of reaction as a function of time for EP_1 and MTHPA is shown in Fig. 3.

The calculated H_{tot} for EP_2 + MTHPA and the blend of system of $EP_1 + EP_2$ is 338 and 364 J/g, respectively. Isothermal runs performed on EP_2 and on the EP_1:EP_2 (1:1) blended sample mixed with the stoichiometric amounts of MTHPA are reported in Figs. 4 and 5, respectively. The curing kinetics follow an autocatalytic model in these cases. As temperature increases, the time required for curing decreases, as expected.

A non-linear least square method was used to determine the kinetic parameters (m, n, and k_2, see Eq. (4)) simultaneously without constraints [49] with Mathematica®. The uncatalyzed reaction rate was estimated from the intercept of the plot at $t = 0$ using the procedure of Dutta and Ryan [50,51]. The comparison of reaction rates for cured systems is presented in Fig. 6. At low temperatures k_1 values for the blend are between those for the pure components while the k_2 results are lower than for the pure components. There are significant differences in k_1 values between EP_1, EP_2 and the blend systems, with the value for the blend much higher. This implies that there are differences in external catalysis mechanisms. However, the k_2 values of these systems are

Table 1
Comparison of kinetic parameters between DGEBP-F/DGEHBP/blend of DGEBP-F and DGE-DHBP systems

Kinetic parameters	DGEBP-F/MTHPA	DGE-DHBP/MTHPA	Blend of DGEBP-F and DGE-DHBP/MTHPA
k_1 (min^{-1})	$1.48\times10^{7}\exp(-8.08/RT)$; $r=0.9908$	$1.52\times10^{11}\exp(-5.83/RT)$; $r=0.9889$	$2.98\times10^{11}\exp(-12.08/RT)$; $r=0.9979$
k_2 (min^{-1})	$2.63\times10^{5}\exp(-5.83/RT)$; $r=0.9871$	$4.03\times10^{6}\exp(-6.88/RT)$; $r=0.9548$	$1.64\times10^{6}\exp(-5.66/RT)$; $r=0.9929$
α_P	$1.24\times10^{6}\exp(-6.78/RT)$; $r=0.9850$	$2.58\times10^{8}\exp(-8.78/RT)$; $r=0.9885$	$3.06\times10^{8}\exp(-8.90/RT)$; $r=0.9970$
t_p (min)	$1.20\times10^{-8}\exp(-8.16/RT)$; $r=0.9962$	$1.97\times10^{-11}\exp(-10.66/RT)$; $r=0.9822$	$2.03\times10^{-11}\exp(-10.64/RT)$; $r=0.9793$
m_{avg}	1.103	1.045	0.995
n_{avg}	1.311	1.216	1.225
Ea_1 (kJ/mol)	67.2	48.4	100.4
Ea_2 (kJ/mol)	48.4	57.2	47.0

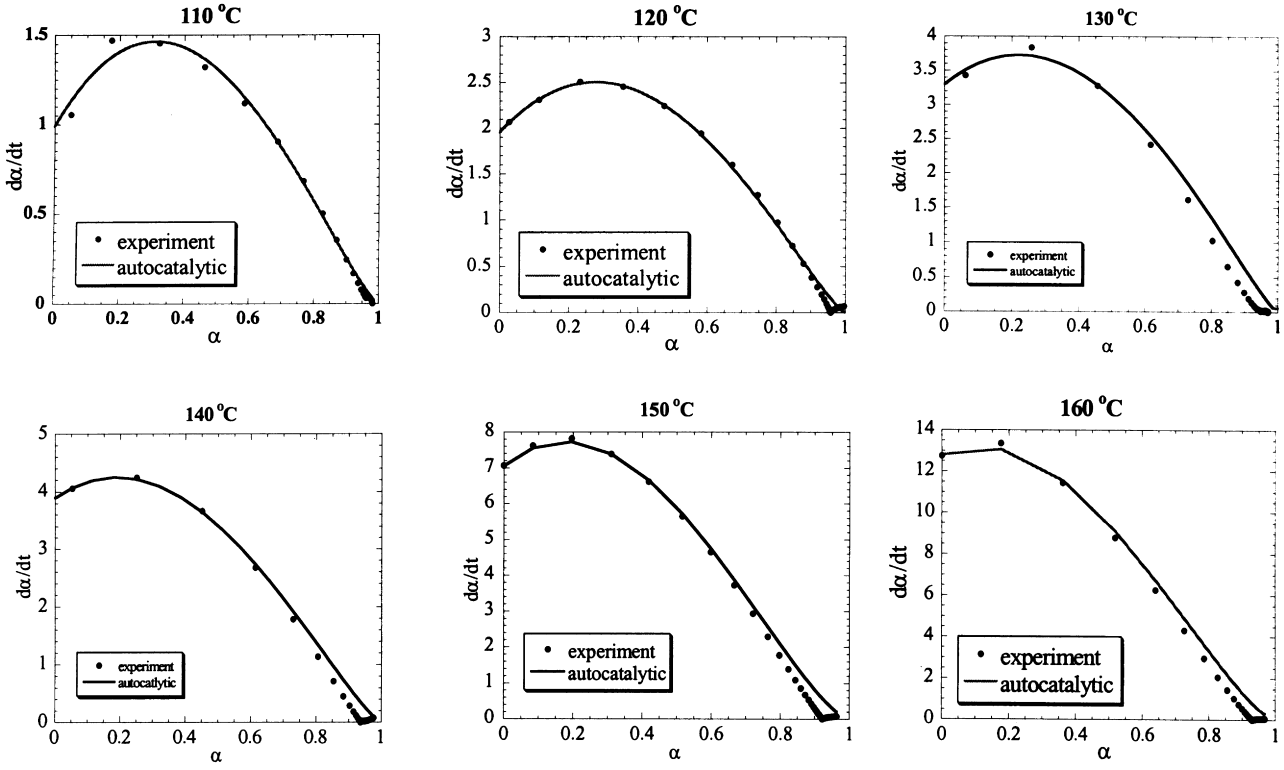

Fig. 8. Comparison of experimental data with autocatalytic model for DGEBP-F and MTHPA system.

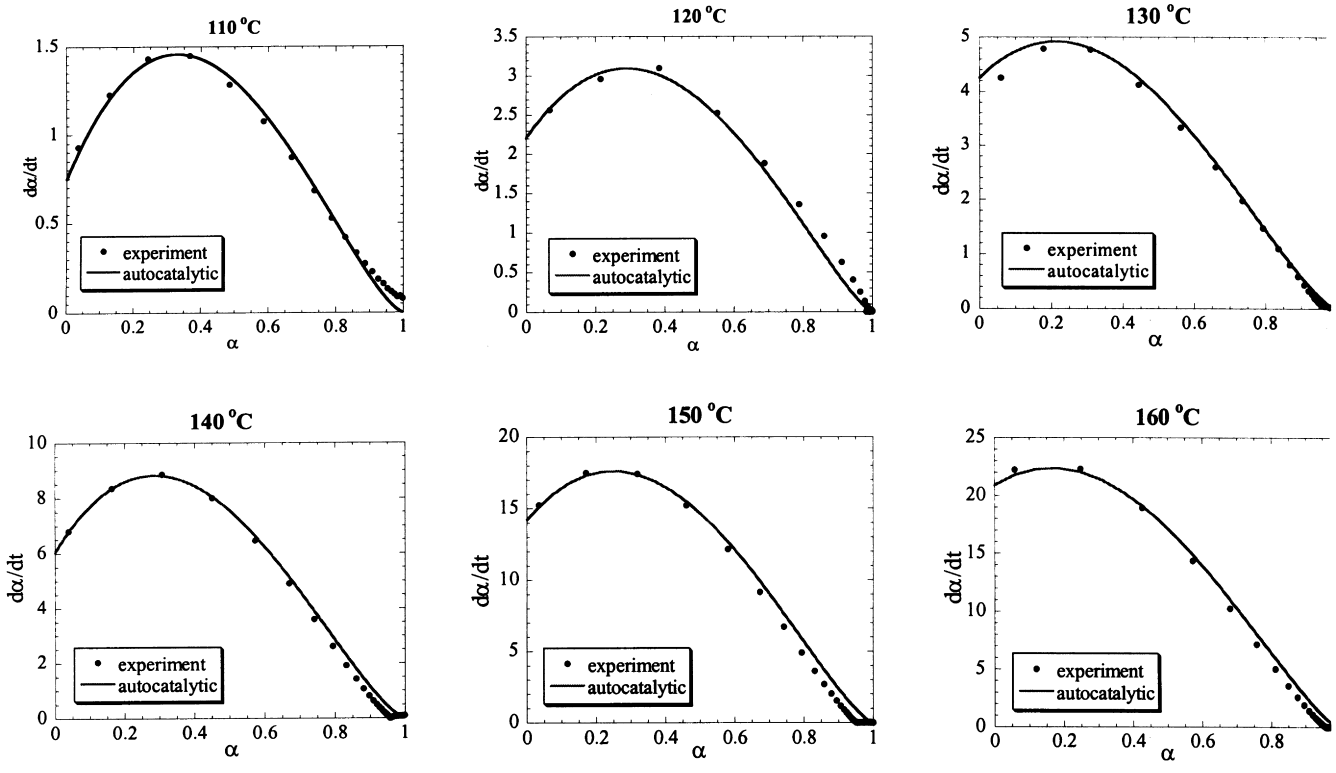

Fig. 9. Comparison of experimental data with autocatalytic model for DGE-DHBP and MTHPA system.

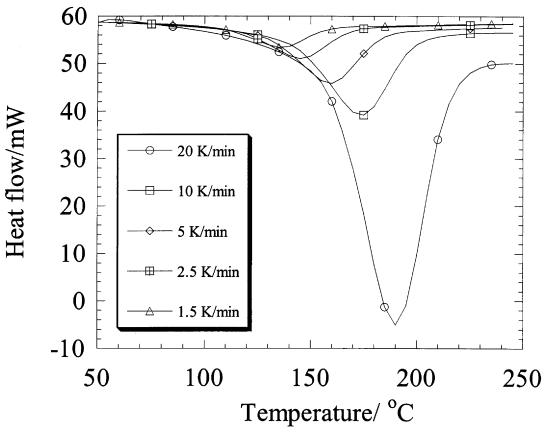

Fig. 10. Dynamic thermogram for different heating rate of DGEBP-F + MTHPA.

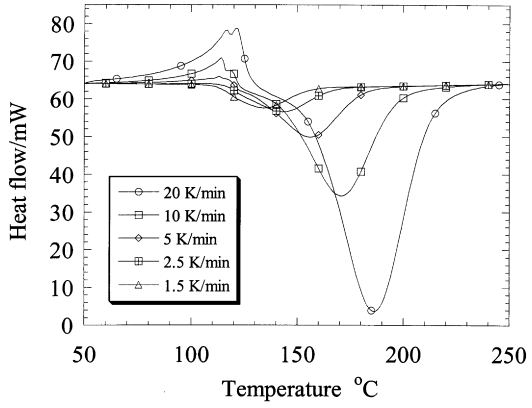

Fig. 11. Dynamic thermogram for different heating rate of DGE-DHBP + MTHPA.

not very different since the reactivity and functionality of both epoxy groups are quite similar.

Fig. 7 shows the comparison of the maximum isothermal reaction rate α_P and the reaction time t_p required to attain the maximum rate. Further, we find that the reaction orders m and n do not change with the temperature, as expected and also as previously observed by Khanna and Chanda [52] for curing of diglycidyl ester with anhydride. Table 1 shows the kinetic parameters for EP_1, EP_2 and the blends of EP_1 with EP_2. The activation energy for curing is obtained from the Arrhenius relationship. Two activation energies are obtained from the autocatalytic model, which represent both the uncatalyzed and the catalyzed curing reactions.

The calculated kinetic parameters were confirmed by fitting the experimental data to the autocatalytic kinetic model, as shown in Fig. 8, for the EP_1 system. Fig. 9 presents a typical comparison between experimental and model results for EP_2 systems. The maximum reaction rate was usually found around 20–40% conversion. The model chosen shows a good fit with the experimental data in the initial stage of reaction and up to about 70% conversion. Deviations are observed near the gelation point; this is expected since the diffusion effect dominates the reaction at higher percentages of conversion [44,45,53].

The non-isothermal thermogram of EP_1 + MTHPA is shown in Fig. 10 and a similar thermogram for EP_2 in Fig. 11. The peak at high heating rate shows the melting before curing reaction. The activation energy is calculated from the slope of the Kissinger relationship. Our E_a values obtained are in reasonable agreement with results of other authors for epoxy + anhydride systems [53–55]. There is a small difference between the activation energies E_a calculated for the systems investigated here, but they follow the same trend as the activation energies for the catalyzed reaction E_{a2} from isothermal kinetics — as displayed in Table 2. The activation energy for the curing reaction of the EP_1 + EP_2 blend is lower compared with the other single-component resin systems indicating that the reaction kinetics of the mixed system are synergistic.

The differences in activation energies for isothermal and non-isothermal analysis for epoxy + anhydride systems has also been investigated by William and co-workers [56]. The effect has been attributed to temperature range difference of curing between isothermal and non-isothermal methods. The chain-wise polymerization mechanisms of epoxies with anhydrides can be divided into three main steps including: initiation, propagation, and chain transfer steps. The tertiary amine base first generates the active sites from anhydride and epoxide groups. These reactive groups further react with epoxy and anhydride as growing chains. The chain transfer step occurs when the active centers are regenerated and growing chains are terminated. The E_a from

Table 2
The non-isothermal data at different heating rates compared between DGEBP-F/DGE-DHBP/blend of DGEBP-F and DGE-DHBP systems

Heating rate (K/min)	Peak temperature (K)		
	DGEBP-F/MTHPA	DGE-DHBP/MTHPA	Blend (DGEBP-F/DGE-DHBP)
1.5	409	408	408
2.5	419	416	418
5	433	429	432
10	447	443	447
20	464	459	464
E_a (Kissinger method) (kJ/mol)	68.2	70.6	65.8

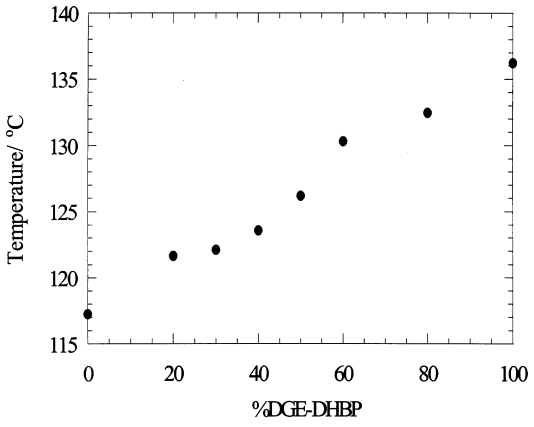

Fig. 12. Comparison of the glass transition temperature of coreacted network vs. DGE-DHBP.

non-isothermal is usually higher than isothermal measurement since the fitting of isothermal DSC is performed after the induction period.

4.3. Glass transition temperature

The glass transition temperature T_g of the coreacted monomer network were evaluated by means of DSC. The relationship between T_g and the composition of the blend sample is shown in Fig. 12. As the EP_2 concentration increases, a single intermediate T_g of the blended samples is observed. With reference to T_gs of the pure system, the T_g of the network increases with DGE-DHBP concentration.

5. Concluding remarks

The DGE-DHBP affects the kinetics of curing DGEBP-F, especially the activation energy of curing. Effects of diffusion control and complicated reactions that retard the basic curing reaction are found in all systems after about 80% conversion. The autocatalytic model does not take into account the effect of mobility retardation after the gelation point. Therefore, the curing rates calculated from the model are higher than the experimental values. The coreacted networks exhibited a single T_g across all compositions, which scaled with increasing DGE-DHBP.

Acknowledgements

Financial support has been provided by the State of Texas Advanced Technology Program (Project#003594-077). Equipment donation by the Perkin–Elmer Corp. is acknowledged also. Comments of the referees and Gale Holmes are appreciated.

References

[1] Kirshenbaum SL. In: Riew CK, editor. Rubber-modified thermoset resins. Washington, DC: American Chemical Society, 1984. p. 163.
[2] Kunz SC, Sayre JA, Assink RA. Polymer 1987;23:1897.
[3] Han X, Yun Z, Guo F. Mater Res Soc Symp Proc 1992;274:11.
[4] Riew CK, Kinloch AJ. Advances in chemistry series 233. Washington, DC: American Chemical Society, 1993.
[5] Prakash NA, Liu YM, Jang BZ, Wang JB. Polym Compos 1994;15:479.
[6] Sperling LH. Interpenetrating polymer networks and related materials. New York: Plenum Press, 1981.
[7] Broer DJ, Finkelmann H, Kondo K. Makromol Chem 1988;189:185.
[8] Ober CK, Weiss RA. Liquid crystalline polymers, ACS symposium series. Washington, DC: American Chemical Society, 1990 (p. 1–13).
[9] Broer DJ, Finkelmann H, Kondo K. Makromol Chem 1989;190:3201.
[10] Broer DJ, Finkelmann H, Kondo K. Makromol Chem 1989;190:2255.
[11] Broer DJ, Lub J, Mol GN. Macromolecules 1993;26:1244.
[12] Onada S, Yano S, Tsunashima K, Inoue T. Polymer 1996;37:1925.
[13] Barclay GG, McNamee SG, Ober CK, Papathomas KI, Wang DW. J Polym Sci Polym Chem 1992;30:1845.
[14] Shiota A, Ober CK. J Polym Sci Polym Chem 1996;34:1291.
[15] Grebowicz JS. Macromol Symp 1996;104:191.
[16] Szczepaniak P, Warchalowska M, Rejdych J, Leszczynska I, Rudnik E. J Polym Sci Polym Phys 1998;36:21.
[17] Sue HJ, Earls JD, Hefner RE. J Mater Sci 1997;32:4031.
[18] Sue HJ, Earls JD, Hefner RE. J Mater Sci 1997;32:4039.
[19] Sue HJ, Earls JD, Hefner RE, Villarreal NI, Garcia-Meitin EI, Yang PC, Cheatam CM, Plummer CG. Polymer 1998;39:4707.
[20] Lin Q, Yee AF, Sue HJ, Earls JD, Hefner RE. J Polym Sci Polym Phys 1997;35:2363.
[21] Carfagna C, Amendola E, Giamberini M. Liq Cryst 1993;13:571.
[22] Brostow W, Hess M, Lopez B, Sterzynski T. Polymer 1996;37:1551.
[23] Brostow W, Sterzynski T, Triouleyre S. Polymer 1996;37:1561.
[24] Brostow W. Polymer 1990;31:979.
[25] Brostow W, editor. Mechanical and thermophysical properties of polymer liquid crystals. London/New York: Chapman & Hall, 1998.
[26] Brostow W, Faitelson EA, Kamensky MG, Korhov VP, Rodin YP. Polymer 1999;40:1441.
[27] Berry JM, Brostow W, Hess M, Jacobs GD. Polymer 1998;39:4081.
[28] Carfagna C, Nicolais C, Amendola E, Carfagna Jr. C, Filippov AG. J Appl Polym Sci 1992;44:1456.
[29] Barclay GG, Ober CK. Prog Polym Sci 1993;18:899.
[30] Muller HP, Gipp R, Heine H. US patent 4,764,581, 1988.
[31] Earls JD, Hefner RE, Puckett PM. US patent 5,218,062, 1993.
[32] Giamberini M, Amendola E, Carfagna C. Mol Cryst Liq Cryst 1995;266:9.
[33] Weiss R, Ober CK, editors. Liquid crystalline polymers: chemistry, structure and properties. Washington, DC: American Chemical Society, 1990.
[34] Carfagna C, Amendola E, Giamberini M, Hakemi H, Pane S. Polym Int 1997;44:465.
[35] Carfagna C, Amendola E, Giamberini M. Prog Polym Sci 1997;22:1607.
[36] Barclay GG, McNamee SG, Ober CK, Papathomas KI, Wang DW. J Polym Sci Polym Chem 1992;30:1845.
[37] Finkelmann H. In: Gray GW, editor. Thermotropic liquid crystals. New York: Wiley, 1987. p. 145.
[38] Jaunder KJ. Organic polymer chemistry. London: Chapman & Hall, 1973.
[39] Fisher RF. J Polym Sci 1960;44:155.
[40] Tanaka Y, Kakiuchi H. J Macromol Sci Chem 1996;A1:307.
[41] Yousefi A, Lafleur PG, Gauvin R. Polym Compos 1997;18:157.
[42] Prime RB. In: Turi EA, editor. Thermal characterization of polymeric materials, vol. 2. New York: Academic Press, 1997.
[43] Lau S. ACS Symposium Series 1992 (p. 496).

[44] Kamal MR. Polym Engng Sci 1974;14:231.
[45] Kamal MR, Sourour S. Polym Engng Sci 1973;13:59.
[46] Kissinger HE. Anal Chem 1957;29:1702.
[47] Carfagna C, Amendola E, Giamberini M, Filippo AG, Bauer RS. Liq Cryst 1993;13:571.
[48] Hefner Jr RE, Earls JD, Puckett PM. US patent 5,266,660, 1993.
[49] Marquardt DN. J Soc Ind Appl Math 1963;11:431.
[50] Dutta A, Ryan ME. J Appl Polym Sci 1979;24:635.
[51] Ryan ME, Dutta A. Polymer 1979;20:203.
[52] Khanna U, Chanda M. J Appl Polym Sci 1993;49:319.
[53] Boey FYC, Qiang W. Polymer 2000;41:2081.
[54] Montserrat C, Flaqué C, Pagés P, Málek J. J Appl Polym Sci 1995;56:1413.
[55] Montserrat C, Flaqué C, Andreu G, Málek J. Thermochim Acta 1995;269/270:213.
[56] Riccardi CC, Dupuy J, Williams RJJ. J Polym Sci Polym Phys 1999;37:2799.